

# *Crossroads of the mesoscale circulation.*

Alberto Baudena<sup>1</sup>, Enrico Ser-Giacomi<sup>1</sup>, Cristóbal López<sup>2</sup>, Emilio Hernández-García<sup>2</sup>, and Francesco d'Ovidio<sup>1</sup>

<sup>1</sup>Sorbonne Universités (UPMC, Université Paris 06)-CNRS-IRD-MNHN, LOCEAN, 4 place JUSSIEU, F-75005 PARIS, France

<sup>2</sup>IFISC (CSIC-UIB), Instituto de Física Interdisciplinar y Sistemas Complejos, Campus Universitat de les Illes Balears, E-07122 Palma de Mallorca, Spain

**Abstract.** Quantifying the mechanisms of tracer dispersion in the ocean remains a central question in oceanography, for problems ranging from nutrient delivery to phytoplankton, to the early detection of contaminants. Until now, most of the analysis has been based on Lagrangian concepts of transport, often focusing on the identification of features that minimize fluid exchange among regions, or more recently, on network tools which focus instead on connectivity and transport pathways. Neither of these approaches, however, allows us to rank the geographical sites of major water passage, and at the same time, to select them so that they monitor waters coming from independent parts of the ocean. These are instead key criteria when deploying an observing network. Here we address this issue by estimating at any point the extent of the ocean surface which transits through it in a given time window. With such metrics we are able to rank the sites with major fluxes that intercept waters originating from different regions. We show that this information leads to the optimization of an observing network, where a set of sampling sites can be chosen so as to maximize the monitored upstream surface. The same analysis, applied instead backward in time, allows us to identify the major sources which feed a target region. The method is applied to the Kerguelen area in the Southern Ocean, using altimetry-derived velocity fields that are validated by observed trajectories of 43 surface drifters, along with statistics on the temporal persistence of the stations determined in this study. We then identify possible hotspots of micro-nutrient enrichment for the recurrent spring phytoplanktonic bloom in the Kerguelen region. Promising applications to other fields, such as larval dispersion or contaminant detection, are then discussed.

## 1 Introduction

Characterizing the evolution of tracers dispersed by the oceanic currents is one of the most important, but still open questions, in oceanography. In some cases it is possible to partially address this point by tracking a given tracer using satellite images, or model simulations, but often *in situ* measurements and adaptive sampling strategies are required. In fact, this is a central question for a number of cases ranging from the retrieval of contaminants and their basins of attraction

(Vrana et al. 2005; Froyland et al. 2014), the sampling of larval dispersal and its connectivity (Bradbury et al. 2008; Planes et al. 2009; Andrello et al. 2013; Melià et al. 2016), the planning of oceanographic surveys (Bellingham and Willcox 1996), to monitoring systems design (Mooers et al. 2005), or characterising and implementing marine protected areas (Rossi et al. 2014; Dubois et al. 2016; Bray et al. 2017).

The horizontal transport at the ocean surface is one of the key mechanisms controlling the dispersion of tracers in the open ocean. Strictly speaking, two main processes contribute to that: mixing, which reduces and smooths the gradients, and horizontal stirring, which instead enhances the tracer gradients (Eckart 1948; Okubo 1978; Garrett 1983; Sundermeyer and Price 1998). Horizontal stirring is one of the main mechanism of turbulence for which an initial homogeneous water mass is stretched by the currents. Consequently, such water masses are shaped in elongated and convoluted filaments, producing a very anisotropic pattern. Filaments can intrude into some regions far apart from their origin, while other areas close to the source location may be shielded by circulation features, the so-called transport barriers. This filamentation process eventually enhances mixing by creating longer contact surfaces between water masses of contrasting properties.

Several tools have been proposed to achieve a better understanding of the role horizontal transport plays in tracer dispersion. Most of these approaches focus on the Lagrangian analysis of the ocean currents based on dynamical system theory (Ottino 1989; Mancho et al. 2004; Wiggins 2005). These methods are mainly devoted to the detection of barriers to transport in flow systems (Boffetta et al. 2001; Abraham and Bowen 2002; d’Ovidio et al. 2004; Prants et al. 2014a,b) or coherent regions (Lehahn et al. 2007; Froyland et al. 2007; d’Ovidio et al. 2013; Berline et al. 2014; Haller 2015; Hadjighasem et al. 2016; Miron et al. 2017) with minimal leaking to surrounding water masses. Interestingly, during the last years, network theory approaches to geophysics (Phillips et al. 2015), flow transport and mixing (Ser-Giacomi et al. 2015a; Lindner and Donner 2017; Fujiwara et al. 2017; Padberg-Gehle and Schneide 2017; McAdam and van Sebille 2018), and turbulence (Iacobello et al. 2018) have also attracted lot of interest.

Recently, some attention has been given to a problem that is complementary and somehow opposite to the identification of transport barriers: how to detect regions that enhance fluid exchanges across a flow system? This issue has been developed particularly in the framework of networks built from lagrangian trajectories (Ser-Giacomi et al. 2015b,c; Lindner and Donner 2017). In such studies, spatial sub-areas of the ocean are represented by network nodes while links parameterize the amount of water exchanged among them. Networks constructed in this way, called Lagrangian Flow Networks (LFNs), provide a topological description of the transport dynamics in the ocean allowing to describe distinct features of the flow by using several network methods. (Ser-Giacomi et al. 2015a; Rodríguez-Méndez et al. 2017; Monroy et al. 2017; Ser-Giacomi et al. 2017).

In particular, it has been shown the existence of localized “bottlenecks” whose presence is responsible for maintaining connections between areas of the seascape

that would be otherwise (almost) disconnected. Borrowing from Network Theory the concept of betweenness centrality, it has been possible to quantify explicitly how much LFN nodes act as bottlenecks for the oceanic flow by counting the number of paths passing through them during a fixed interval of time (Ser-Giacomi et al. 2015b).

The main limitation of the betweenness centrality, however, is that it identifies bottleneck regions that, even if topologically relevant for the connectivity geometry, do not present a flux necessarily important in terms of volume. This is related to the fact that betweenness is measuring the number of connections crossing a node, regardless of connectivity strength. Therefore, to pinpoint hotspots that maximize the incoming or outgoing flux in a given time window, one should focus on strong “passage points” of water, instead of only topological bottlenecks.

In this paper we aim to detect these hotspots, which act as “crossroads” of the circulation, being traversed by the largest amount of water coming from (or going to) a focal region. This is achieved by examining the trajectories that pass by during a given time period. This calculation provides a quantity, which we call *crossroadness*, which is the surface flow through each spot of the domain considered in a specific temporal window.

Moreover, our calculation preserves the information on the original location of each passing trajectory. Based on *crossroadness* analysis, we introduce thus an algorithm for designing a sampling network with minimal redundancy, i.e., in which the flow of a given source region through the observing network is maximized and the number of stations minimized. This algorithm may be important in contaminant retrieval or strategies aimed at the analysis of the largest surface possible.

Reversing the analysis backward in time, we can use the same method to find the major “source” points from which the water distributes over a target area, each source “irrigating” independent sites. This may be relevant to rank monitoring importance of sites feeding water to a sensible region, for instance a marine protected area.

We note that in a recent paper, Rypina and Pratt (2017) introduced a “mixing potential” approach which exploits ideas similar to our *crossroadness*. The main difference is that the *mixing potential* is a Lagrangian quantity attached to each fluid parcel, whereas *crossroadness* uses Lagrangian trajectories but it is assigned to each fixed location in space. Thus, whereas the diagnostic in Rypina and Pratt (2017) may be more appropriate to assess mixing, we are more interested in algorithms to deploy observation networks and identify sources of transported substances.

The paper is organized as follows: Sec. 2 describes the methodological assumptions and the dataset employed for the computation and the validation of the results. In particular, Subsec. 2.3 introduces the *crossroadness* and its oceanographic interpretation. We then determine a ranking method (Subsec. 2.4) that provides the sites with the major passage of water dispersed from a source region or feeding a target region, when computed forward or backward

in time, respectively. Validation and case studies are then described in Sec. 3. In Subsec. 3.1, the method is applied to satellite altimetry data and validated against the trajectories of real SVP drifters in the Southern Ocean. In Subsec. 3.2, the relationship between the surface being monitored and the number of stations employed is examined. An analysis of the persistence of the observing network is in Subsec. 3.3. In Subsec. 3.4, we use the method to identify possible sites from which nutrients are delivered offshore the Kerguelen plateau, fuelling the open ocean planktonic bloom. A summary of the results, along with an illustration of the perspectives and possible fields of application is given in the Discussion (Sec. 4). Finally, our paper is completed by two appendices, extending the analysis of the sensitivity of our diagnostic to changes in the dates of the velocity field used (Appendix A), and giving some link of our new diagnostic, under particular hypotheses, to averages of velocity and of kinetic energy (Appendix B).

## 2 Data and Methods

We adopt a Lagrangian approach by studying the transport properties of the ocean using particle trajectories. Lagrangian trajectories are computed over a grid of initial conditions by integrating surface ocean currents derived from satellite altimetry. We focus, in particular, on the Kerguelen region of the Southern Ocean, where in 2011 the KEOPS2 campaign released, over 20 days, an array of 48 surface drifters. We use a set of stations, defined by our method, for a virtual “search and rescue” of these drifters. This is an ideal case study for validating the capacity of the algorithm presented here to identify points with enhanced passage of particle trajectories. The Kerguelen region is also characterized by a spring-time phytoplanktonic bloom preconditioned by the redistribution of micro-nutrients (in particular iron) advected by the Antarctic Circumpolar Current (ACC) from the Kerguelen plateau margin out into the open ocean (d’Ovidio et al. 2015). Satellite-derived chlorophyll is therefore a useful tracer of transport pathways, and an opportunity for pinpointing likely sources of iron by employing the theoretical concepts developed in this paper.

We present in the following subsections the multi-satellite products employed, the details of the trajectory computation and the SVP drifters.

### 2.1 Altimetry and Chlorophyll data

For the velocity field we use the DUACS (Data Unification and Altimeter Combination System) delayed-time multi-mission altimeter gridded products defined over the global ocean with a regular  $\frac{1}{4} \times \frac{1}{4}^\circ$  spatial sampling (Pujol et al. 2016) and available from the E.U. Copernicus Marine Environment Monitoring Service (CMEMS, <http://marine.copernicus.eu/>). An experimental regional product is also considered. It corresponds to the regional Kerguelen product, velocities computed from altimetry in delayed time on a regular  $\frac{1}{8} \times \frac{1}{8}^\circ$  grid and available from Aviso (<http://www.aviso.altimetry.fr/duacs/>).

The field of chlorophyll was downloaded from the Oceancolour product (OCEAN-COLOUR\_GLO\_CHL\_L4.REP.OBSERVATIONS.009.082) at CMEMS. These data are provided by a map computed from satellite observations over a period of 8 days (to limit cloud coverage), and with a spatial resolution of  $4 \text{ km} \times 4 \text{ km}$ .

## 2.2 SVP drifters

During the KEOPS2 campaign in October-November 2011, 48 Surface Velocity Program (SVP) drifters were released within the Kerguelen region. The SVP drifting buoy is a Lagrangian current-following drifter, composed of a spherical surface float of 35 cm in diameter, which contained the battery, a holey sock drogue of about 6 meters, that tracked the water currents at a nominal depth of 15 m, representative of the surface circulation, and a satellite transmitter which relays the data through the Iridium system. All the buoys address the World Ocean Circulation Experiment (WOCE) benchmarks.

In our study we consider only the drifters released at a longitude greater than  $68^\circ\text{E}$ , i.e. on the eastern part of the Kerguelen plateau. The remaining drifters do not cross the plateau because they are advected westward, and are not useful for our purposes. We therefore consider 43 drifters trajectories of the 48 drifting buoys originally deployed. We assume the 11th of November 2011 as the release date. The duration of the trajectories ranges between 63 to 93 days (average of 81 days), with a temporal resolution of 1 day.

## 2.3 The crossroadness: characterizing regions by the amount of water crossing them

In order to characterize the dispersion process of a tracer, we want to assess which are the points that highlight the advection history of a given patch. We define thus a new quantity, that we call *crossroadness* (CR), measuring the ocean surface crossing a region of a given size in a fixed temporal window. To do that, we consider two grids, both of angular cell size  $\delta$ , where each cell has a point in the middle.

In the first grid, the *initialization grid*, the central points are advected forward in time with DUACS altimetric velocities with a 4th order Runge-Kutta integration scheme, for a period between 30 and 90 days and a time step of 3 hours. Each trajectory thus computed contains 8 points per day ( $N_{PT} = 8 N_D$  in total,  $N_D$  number of days). The initial angular separation between two contiguous particles ( $\delta$ ) used in the computations, varies from 0.1 to 0.4 degrees. By initial separation  $\delta$  we mean the difference in latitude among contiguous rows of particles. Along the longitudinal (LON) direction, to keep the same distance, the separation is corrected by the cosine of the latitude LAT ( $\delta_{LON} = \delta / \cos(LAT)$ ). In this way, all the cells have the same lateral sizes,  $R\delta$ , and area  $\Delta = R^2\delta^2$  (with  $\delta$  in radians, and  $R$  the Earth radius).

Over each point  $\mathcal{P}$  of the second grid (constructed in the same way as the initialization one, and referred to as *observational grid*) we compute the crossroadness as follows. We count the number of trajectories passing below an angu-

lar distance  $\sigma$  from  $\mathcal{P}$ . This is done by computing the spherical distance between  $\mathcal{P}$  and the first point of the trajectory, then the second one, the third one and so on. We obtain thus  $N_{PT}$  values. We consider as distance between the trajectory and  $\mathcal{P}$  the minimum among the  $N_{PT}$  values. With  $\sigma$  in radians, the value  $R\sigma$  represents the neighborhood radius (the detection range) of each point in the observational grid. As the dimensions of a cell in the *initialization grid* are relatively small, we can consider that the trajectory is representative for the whole content of the box from which it is originated (therefore,  $\sigma \geq \delta$ ). Thus, if we multiply the number of trajectories counted times the surface of a cell,  $\Delta$ , we will obtain an estimation of the total water surface that passed through the node during the period  $\tau$ . We call this total water surface flowing inside the detection range  $\sigma$  of the point  $\mathcal{P}$  the “crossroadness” (or “CR”) at  $\mathcal{P}$ . In this way we define a CR field on all points of the observational grid. Because of the quasi-twodimensional nature of ocean circulation at the scales considered here, the amount of surface is proportional to the volume and then to the mass of the water transported in the upper ocean layers. A representative scheme of this concept is present in Fig. 1, where the crossroadness of the point in the circle is  $3\Delta$  since there are three trajectories entering its observational range. The same procedure can be applied backward: the *initialization grid* is advected backward in time, and, over the *observational grid*, we count for each point how many trajectories pass below the detection range  $\sigma$ . In this way we obtain the crossroadness backward in time.

## 2.4 Ranking method for the optimization of a network of CR stations

In the study of the dispersion of a passive tracer one of the main questions is the definition of an effective sampling strategy. Considering the tracer (e.g. a contaminant) with a finite life time, we want to know what would be the best distribution of monitoring sites (referred to as “stations”) that can intercept the largest fraction of the advected tracer. In a turbulent pattern of circulation, the answer to this question is not obvious, since the patch can be redistributed irregularly through the domain considered.

Sampling on a regular grid is a possible choice. However, depending on the circulation patterns, we can easily imagine that some retrieving sites may convey water from larger regions than others. The diagnostic introduced above provides implicitly a simple method for the definition of a sampling strategy. In fact, if we want to choose the best monitoring station, we will simply select the site crossed by the largest number of trajectories originated by the source region of the tracer, i.e. the one with the higher value of crossroadness. In order to define the second most important monitoring station, we exclude the trajectories already monitored by the first station. We consider only independent trajectories, i.e. originated from different locations of the *initialization grid*, and we determine also the second station. Proceeding in this way we identify a network of *CR stations* (Fig. 2).

The calculation can be performed backward in time as well. The initialization

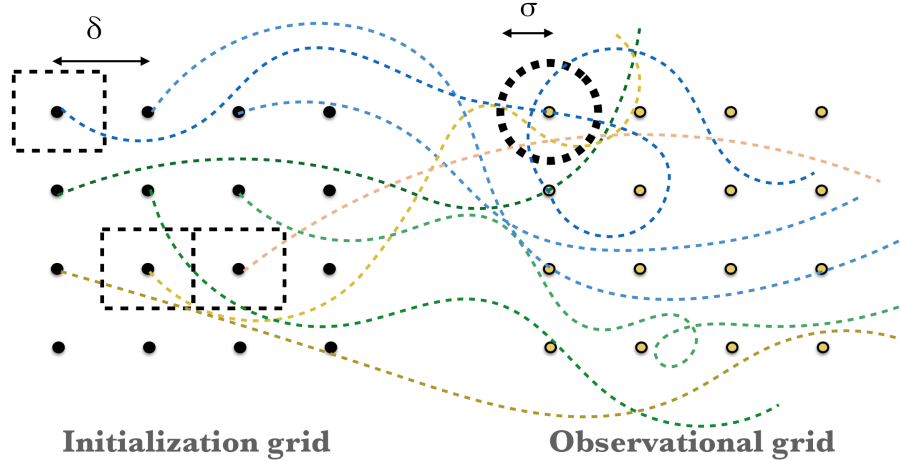


Fig. 1: Illustrative example for the calculation of the crossroadness. Colored dotted lines correspond to different trajectories originating from the *initialization grid* (left), advected for a time  $\tau$ . The circle (thick dotted line) represents the detection range of the station of the *observational grid* (right), while the rectangles (thin dotted line) contain the surface of water that passes through the station.

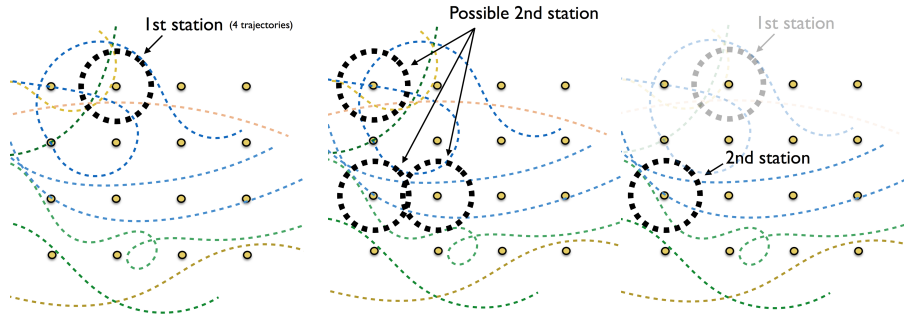


Fig. 2: Illustrative scheme for the determination of the position of a network of observing stations which maximize the detection of a dispersed tracer. The first station is the one that collects the largest number of trajectories, in this case the one circled in the left panel (4 trajectories). Then, we have 3 possible second stations, each with 3 trajectories passing near them (middle panel). But since we consider only independent trajectories, we have to exclude the ones already sampled by the first station (panel on the right). In this way we have only one second possible station.

region becomes a target region. In this case, the network of CR stations represents the ensemble of locations which maximize the surface water feeding the target region.

### 3 Results

#### 3.1 SVP drifters and crossroadness in the Kerguelen region

In order to test the crossroadness and the ranking method as defined in Subsec. 2.3 and 2.4, we use the dataset from the KEOPS2 campaign, in which 43 drifters were released in a relatively small area (the eastern margin of the Kerguelen plateau), approximately in the same period of time (around the 11th of November 2011), and advected for a similar window of time (81 days on average) by the currents, as shown in Fig. 3. We use thus 43 real drifter trajectories.

The regions of densest passage of these real buoys will then be compared with the ones predicted by the CR method, which is obtained from the advection of the *initialization grid*. The former consists in a series of virtual tracers displaced in the following way. We consider the region of release of the real drifters (between  $[-51, -47]^{\circ}\text{S}$ , and  $[70, 75]^{\circ}\text{E}$ ). We cover it with rows of virtual tracers, separated by  $\delta = 0.1^{\circ}$  along the latitude. In order to preserve the same angular distance ( $0.1^{\circ}$ ) among tracers of the same row, we make a latitudinal correction on their longitudinal separation, so that  $\delta_{LON} = \delta / \cos(LAT(row))$ , as explained in Subsec 2.3. We put in each row the same number of tracers.

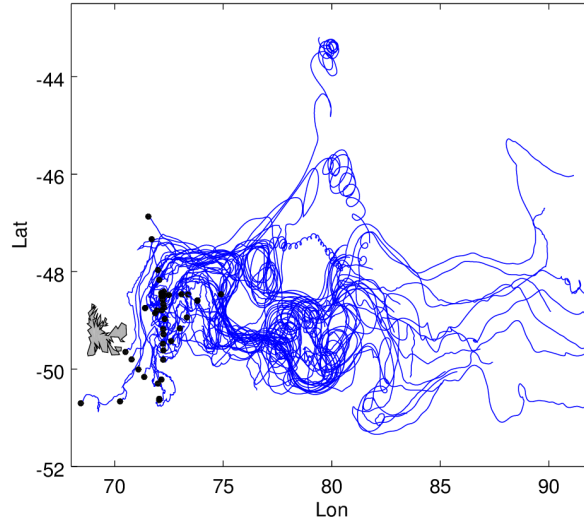


Fig. 3: Trajectories of the 43 drifters of the KEOPS2 Campaign. Black dots represents the starting positions of the drifters.

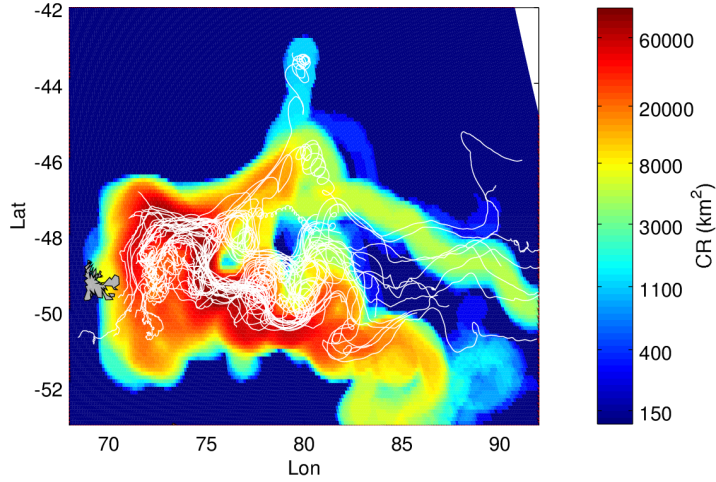


Fig. 4: Crossroadness field derived from satellite altimetry ( $\tau = 60$  days,  $\delta = 0.1^\circ$ ,  $\sigma = 0.4^\circ$ ), with superimposed trajectories of SVP drifters released during the 2011 KEOPS2 campaign. The CR field was computed advecting only the small *rectangle* (longitude:  $[70, 75]^\circ$ ; latitude:  $[-51, -47]^\circ$ ) in which the drifters have been released.

Thus, the longitude range of the southern row (at latitude  $51^\circ\text{S}$ ) is  $[70, 75.4]^\circ$ . For simplicity we will denote in the following this type of geographic region as a *rectangle* of coordinates longitude= $[70, 75]^\circ$  and latitude= $[-51, -47]^\circ$ . We use the altimetry-derived velocities to advect these points forward in time for a period of  $\tau = 60$  days. We compute the CR values at all points separated by the same distance  $\delta$  on the Kerguelen region, i.e. a *rectangle* of boundaries longitude= $[68, 92]^\circ$  and latitude= $[-53, -42]^\circ$ , which constitutes our *observational grid*. The resulting CR field is displayed in Fig. 4. We see a remarkably good agreement between features in the drifters trajectories and the ones in the CR field: areas of denser buoy passage correspond with higher values of the field, suggesting a good qualitative match between CR high values and areas of drifters passage. More quantitative results are obtained by considering a set of 6 best-ranked CR stations (the choice on the quantity of stations is arbitrary) with the method explained in the previous section. The number of real drifters intercepted by the CR stations is compared to the result obtained by a set of stations placed on a regular grid. This last set is constituted by  $3 \times 2$  stations distributed over the area of the drifters motion, separated longitudinally by  $2.5^\circ$  and  $1.23^\circ$  latitudinally.

The measure is repeated several times and for different parameters, changing the advection time  $\tau$  (at 30, 60 and 90 days), the detection range  $\sigma$  (at 0.1, 0.2 and

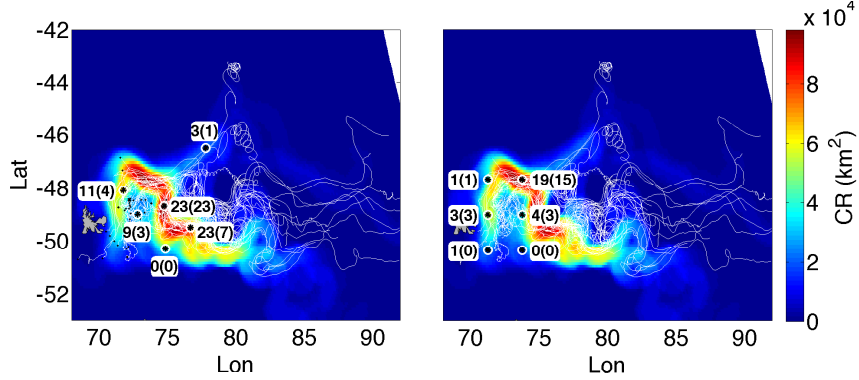


Fig. 5: Left panel: first 6 CR stations (black stars) superimposed on the CR field computed advecting the same region as in Fig. 4, using the regional product for the velocity field ( $\tau = 60$  days,  $\delta = 0.1^\circ$ ,  $\sigma = 0.2^\circ$ ). Right panel: same CR field, this time the black stars identify 6 stations disposed on a regular grid. For each station, the first number identifies the amount of total drifters intercepted, the value in brackets the number of independent drifters. Amount of drifters intercepted by the CR stations (total and in parenthesis the independent): 69 (38). Regular grid: 28 (22).

**Drifters Intercepted**

	CR Stations		Grid
	Global product	Regional product	
$\sigma=0.1^\circ$	30.5(25.5)	30.0(23.5)	12.0(11.0)
$\sigma=0.2^\circ$	53.0(34.0)	68.3(37.3)	28.0(22.0)
<b>Total mean</b>	<b>41.2(30.6)</b>	<b>51.0(31.8)</b>	<b>21.6(17.6)</b>

Table 1: Number of drifters intercepted (out of 43) using six CR stations (left columns) or six stations disposed on a  $3 \times 2$  regular grid. The value is an average obtained changing the different parameters used (the advection time  $\tau$ , the detection range  $\sigma$  and the resolution of the initialization and observational grids  $\delta$ ). For each cell, the two values correspond respectively to the total number of drifters intercepted by the stations and, in parenthesis, to the independent ones. First column: global product for altimetric velocities. Second column: regional product. Third column: stations on a regular grid.

$0.4^\circ$ ) and the resolution of the initialization and observational grids  $\delta$  (at  $0.1$  and  $0.2^\circ$ ). An illustrative example is reported in Fig. 5, where  $\sigma = 0.4^\circ$ ,  $\delta = 0.1^\circ$  and  $\tau = 60$  days.

For each station, the total number of intercepted drifters is computed, as well as the number of drifters first detected by this station (independent ones). The re-

sults are reported in Table 1. The first two columns show the number of drifters (total and independent) intercepted with the CR stations, the third one the values obtained with a regular grid. The efficiency of our method is about twice the result obtained with a regular grid. A lower value of sigma corresponds not surprisingly to a lower number of catches for both the CR and the regularly spaced observing grid, but to an improved ratio in favor of the CR network.

### 3.2 Dependence of the surface monitored on the number of monitoring CR stations

We present here a statistical analysis aimed at assessing the skill of a detection network based on the crossroadness with respect to a set of stations randomly chosen or arranged on a regular grid. The benchmark that we use is the CR, i.e. the ocean surface crossing the CR observing network as a function of the number of the monitoring stations.

Figure 6 displays a map of forward crossroadness computed around Kerguelen Island, advecting particles starting from November 1st, 2011, for a time of 60 days. Superimposed, white circles identify the first four CR stations. Black dots

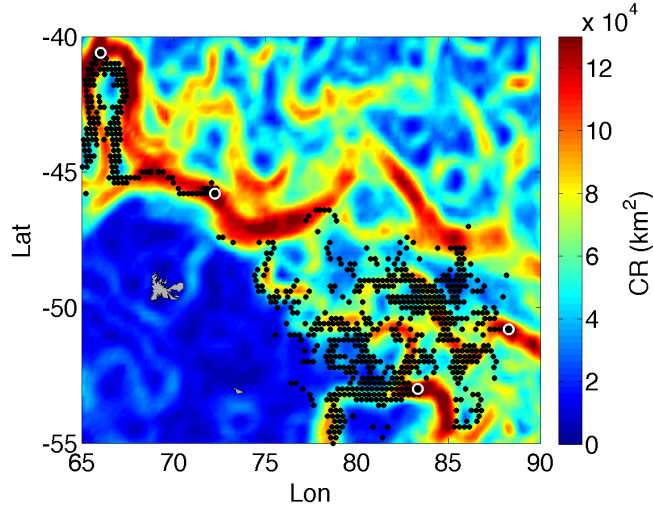


Fig. 6: For this plot and the ones showed in Appendix A, the advected area is the *rectangle* between longitude=[55, 100]°, latitude=[-36, -59]°, while the CR was computed only in the observational domain showed, if not specified differently. Crossroadness computed with an advection time  $\tau = 60$  days,  $\delta = \sigma = 0.2^\circ$ , with, superimposed, the first four CR stations (white circles) and the surface that they control (black dots on the corresponding initialization grid points). Note that some black dots can be outside the plot, since we advected a larger region than the observational domain showed in the panel, in order to take into account the particles upstream.

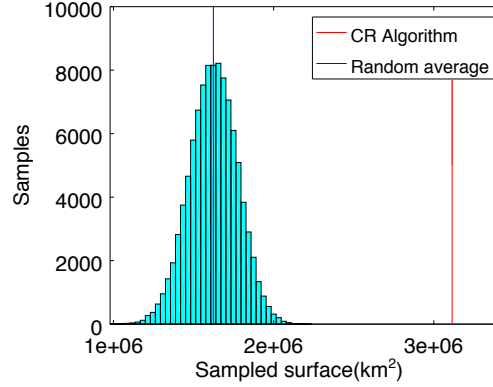


Fig. 7: Histogram, computed from 100000 experiment repetitions, of the surface detected choosing each time  $N = 20$  stations randomly displaced. The vertical red line on the right is instead the surface scanned choosing the stations with our CR algorithm. Here  $\sigma = 0.4^\circ$ . The distance between the mean value of the distribution (vertical blue line) and the vertical red line is 9.96 times the standard deviation of the distribution.

identify the monitored waters, namely the points that will pass in proximity of one of the four stations during the advection time  $\tau$ .

In order to provide a statistical analysis, first we measure the surface monitored by 20 randomly selected stations with a detection range of  $0.4^\circ$  in a period of 60 days. The measure is repeated 100000 times and the results are reported in the histogram of Fig. 7. The vertical blue line is centered on the mean value of the distribution, while the red one is the value of the surface scanned with 20 stations chosen with our method. The distance between the two measures is about ten times the value of the standard deviation of the distribution, an extremely significant ( $p < 10^{-22}$ ) deviation with respect to the expected result of monitoring a larger surface with randomly selected stations.

The measure is repeated changing the number of stations selected, and the results are shown in Fig. 8. A sampling with a regular grid is performed as well. In this case, each measure is obtained by rigidly shifting the grid by a random fraction of the grid step along longitude and latitude. The use of the CR stations (blue dots) shows a better performance compared to the regular grid (black stars) and the random case (red circles) sampling. E.g., to scan a surface of  $3 \times 10^6 \text{ km}^2$  with a sampling power of  $R\sigma = 40 \text{ km}$ , 25 stations selected with the CR method are needed, about 55 with a regular grid, and 75 randomly chosen.

### 3.3 Persistence of the monitoring network

The calculation of the crossroadness computed in the previous sections requires that at the moment of choosing the monitoring stations, the velocity that will

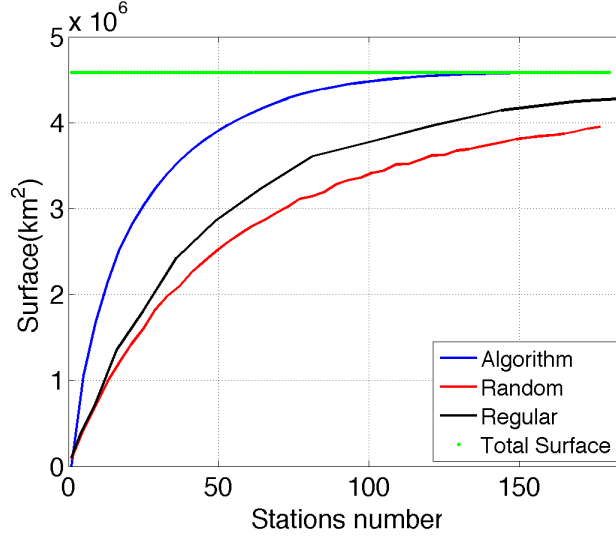


Fig. 8: Surface sampled varying the number of stations considered ( $\tau = 60$  days,  $\delta = 0.1^\circ$ ,  $\sigma = 0.4^\circ$ ), chosen randomly (red line), on a regular grid (black line) and with the CR method (blue line). Concerning the random choice and the regular grid, each value was obtained from the average of 1000 repeated measures. For the case of the regular grid, each time it was rigidly shifted along the longitude and the latitude of a random fraction of the distance between two grid points. The green line represents instead the total surface.

disperse the tracer in the future is already known with good precision. As an example, in Subsec. 3.1 we calculated the CR stations used to intercept the SVP drifters using the velocity data referred to the days in which the buoys were advected by the currents. How much this requirement impacts the CR stations ability to intercept the maximal surface of a stirred patch? Here we attempt to address this question by studying the “persistence” of the CR stations. This means studying what are the consequences on the capacity of a CR network, computed using velocity data of the past, when it is used to intercept a tracer dispersed in the near future.

*Surface monitored using past velocity field for the computation of the CR stations.*

In general, we define

$$\mathcal{T}(\mathcal{R})_{D_0 \rightarrow D_f}$$

as the whole collection of trajectories  $\mathcal{T}$  generated from the advection of all the points regularly initialized over a region  $\mathcal{R}$ , from the day  $D_0$  until  $D_f$ . In general, from a set of trajectories  $\mathcal{T}(\mathcal{R})_{D_0 \rightarrow D_0 + \tau}$ , we can compute an ensemble of CR stations  $\mathcal{S}(\mathcal{R})_{D_0 \rightarrow D_0 + \tau}$ , as explained in Subsec. 2.4, that will be for construction the best choice in order to scan  $\mathcal{T}$ .

When the velocity field between the day  $D_0$  and  $D_0 + \tau$  is not known, we can use the stations computed with the velocity field in a time interval previous to  $D_0$ , e.g.  $\mathcal{S}(\mathcal{R})_{D_0-\tau \rightarrow D_0}$  to monitor the area, under the assumption that if the flow does not change much in an interval of time of the order of  $\tau$  the optimal stations will maintain approximately the same positions.

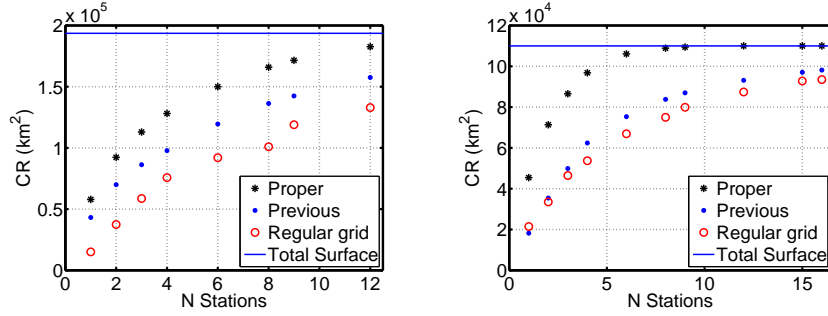


Fig. 9: CR, i.e. surface monitored as a function of the number of stations. Each point is the average obtained changing  $D_0$  over the first day of each month of 2011. Black stars represent the value obtained using the stations computed with the proper velocity field, i.e.  $\mathcal{S}(\mathcal{R})_{D_0 \rightarrow D_0+\tau}$ , while blue dots the ones computed with the previous  $\tau$  days, (i.e.  $\mathcal{S}(\mathcal{R})_{D_0-\tau \rightarrow D_0}$ ). Red circles are the values obtained with a regular disposition of the sampling sites. Left panel:  $\mathcal{R} = \mathcal{R}_P$  (plateau region). Right panel:  $\mathcal{R} = \mathcal{R}_T$  (turbulent area).  $\delta = 0.2^\circ$ ,  $\tau = 60$  days,  $\sigma = 0.2^\circ$ .

Thus, in this section we use the velocities between  $D_0 - \tau$  and  $D_0$  to compute a set of stations  $\mathcal{S}(\mathcal{R})_{D_0-\tau \rightarrow D_0}$ . We use then the latter to monitor  $\mathcal{T}(\mathcal{R})_{D_0 \rightarrow D_0+\tau}$  and see how many trajectories (i.e. sea surface) they intercept.

We take as  $D_0$  the 1st January, 2011 and  $\tau = 60$  days. We change the number of stations considered between 1 and 16, analogously to what has been done in Subsec. 3.2. For comparative purposes, we also measure the surface intercepted with  $\mathcal{S}(\mathcal{R})_{D_0 \rightarrow D_0+\tau}$ , and then with a regular disposition of the stations. We then repeat the procedure using as  $D_0$  the 1st February 2011, then the 1st March 2011 and so on, until the 1st of December 2011 and we consider the average of the 12 values obtained. In this way we obtain a more consistent statistics.

The results are reported in Fig. 9. We consider two different monitoring areas: the first one is the drifters release area, defined in Subsec. 3.1, situated mainly on the Kerguelen plateau and in which the bathymetry seems to affect the circulation pattern, making it more persistent in time. We will refer to it as  $\mathcal{R}_P$ . We then consider a more turbulent region situated offshore from Kerguelen, in which the current field should not be as constrained by the shallow shelf structures as in the former case, and in which the mesoscale structures affect deeply the variability of the currents (Park et al. 2014). We take this turbulent

region  $\mathcal{R}_T$  to be the *rectangle* with longitude between  $80$  and  $83^\circ E$ , and latitude between  $47$  and  $50^\circ S$ .

Concerning the plateau region (left panel in Fig. 9), we see a stronger performance of the CR stations compared to the regular grid, even if they are computed with the trajectories of two months before. E.g., in order to monitor a surface of  $100000 \text{ km}^2$ , we need 8 stations disposed regularly, while only 4 if we consider the stations obtained from the advection of the previous 60 days, and 3 if we consider the advection from time  $D_0$  (i.e. the velocity field simultaneous to the surface advection).

The results are worse but surprisingly consistent for the turbulent region scenario (right panel in Fig. 9), with about 25% less CR stations needed than in the regular case. The analysis in this section is completed in Appendix A, in which the detection power of the CR stations is assessed against further changes in the dates used for the velocity field.

### 3.4 Identification of a source region

In the previous section we used the crossroadness for intercepting a tracer stirred from a given region. Here instead we study another typical problem arising when studying dispersion, namely the identification of the most important source regions connected by the circulation to a given target area.

This issue occurs, for instance, when determining the key regions that can affect vulnerable marine protected areas downstream, or in the identification of nutrient sources feeding a biogeochemical active region (Ciappa and Costabile 2014; Suneel et al. 2016).

In order to showcase this application, we considered the area studied in the previous section, i.e. the Kerguelen plateau, that recent studies have stressed as a natural source of iron supply that sustains the primary production in the zone situated to the east of the island (d'Ovidio et al. 2015; Blain et al. 2008; Christaki et al. 2008).

Large areas of the Earth oceans present waters with high quantities of nutrients, but low concentration of chlorophyll (HNLC). This is generally due to the absence of some micronutrients that act as limiting factors. In many cases one of the main constraints to the presence of chlorophyll is the low concentration of bioavailable iron. In this regime, injection of this micronutrient fuels the primary production (Boyd et al. 2007; Lam and Bishop 2008; Martin et al. 2013). In recent years, different studies have underlined the importance of continental margins as a subsurface source of iron that can thus feed the phytoplanktonic bloom in the waters downstream (Lam and Bishop 2008). Among them, the Kerguelen plateau is one of the clearest region to show this biogeochemical dynamics and its importance for primary production is now well established. Nevertheless, the hotspots of the continental shelf that may act as main iron sources are still unknown. Here we use the crossroadness computed backward in order to address this question.

Since we want to determine the possible iron sources on the Kerguelen plateau, delimited by the bathymetric line of 1000m, we examine only the region

situated eastward to this contour. This is approximated by considering only a region delimited by the perimeter reported in Fig. 10 (left panel, black dotted line). Furthermore, in order to consider only the waters that support a spring-time bloom, we analyze satellite-derived images of the chlorophyll patch of spring 2011. We therefore consider as starting points only the pixels that, belonging to the area enclosed by the perimeter, present at least one value of chlorophyll concentration larger than  $1 \text{ mg/m}^3$  during the peak of the bloom of November and December 2011. Note that, in this way, we do not have an *initialization grid*, but a set of initialization points. The selection is reported on the left panel of Fig. 10 (red points). These points are advected backward for a period of time  $\tau = 180$  days, and the crossroadness field is reported in Fig. 10 (right panel). This map highlights a strong passage of water coming from the northern part of the plateau, underlining the central role of the Antarctic Circumpolar Current (ACC) in the advection of waters in proximity of the island platform, and shows also the Southern ACC Front (SACCF) that passes into the Fawn trough. We then use the ranking algorithm in order to locate the most important passage points which feed water to the blooming region. The first three CR stations are all in proximity of the northern part of the plateau, meaning that in the 180 days before the bloom, the largest part (about 70 %) of the water that will sustain primary production, passed in these three points. This analysis locates the Gallieni Spur as a strong candidate where to search for iron sources of the Kerguelen bloom. We note that in general our CR algorithm does not really

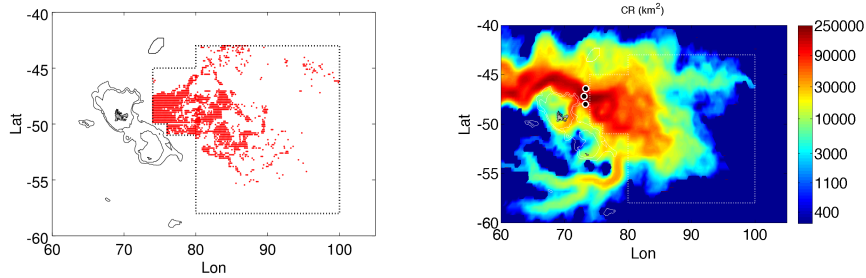


Fig. 10: Left panel: Kerguelen plateau with the bloom area delimited by black dotted lines. Bathymetric lines at 500 and 1000 meters. The set of initializing points (shown in red) are selected by choosing the pixels that supported at least one value of chlorophyll greater than  $1 \text{ mg/m}^3$  between November and December 2011 and are showed in red. Each initialization point is assumed to carry an amount of water given by a surface  $\Delta = R^2 \delta^2$  (when  $R$  is the Earth radius and  $\delta$  is in radians) for  $\delta = 0.15^\circ$ . Right panel: CR computed backward (in log scale), with advection time  $\tau = 180$  days, from the red points showed on the left panel, that presents a total area of about  $517000 \text{ km}^2$ . Black dots represent the first three source stations computed with the CR algorithm described above. Detection range  $\sigma = 0.4^\circ$

determine *source* regions, but rather regions of dense trajectory passage. But since half lifetime of iron in these waters is of the order of about two-three weeks (d’Ovidio et al. 2015), for the value of  $\tau$  used our method in this case should also locate source regions.

## 4 Discussion and perspectives

When studying dispersion problems, in particular at scales related to the dispersal of contaminants ( $\sim 10 - 100$  kms), two main questions arise.

From one side, we have the case of a passive tracer, advected by the currents. The chaotic and turbulent dynamics characterizing the ocean circulation can disperse the patch and make it spread over a large area (say, of size larger than 100 km) within a short time (days to weeks). In this case, a recurrent problem is to locate the sites where to deploy observing stations, capable of monitoring or collecting the dispersed tracer.

A second class of problems concerns the case of a sensible region that is influenced by the circulation upstream. In this case, the identification of the “sources” that may affect and spread all over the target area is important for vulnerability assessment.

Current methods, mainly based on Lagrangian advection of particles, concern mostly the identification of coherent regions with minimal transfer of water toward the environs: nevertheless, the knowledge of the spots that instead enhance the exchanges amongst a flow system is a central issue in dispersion problems. The latter question has been recently addressed in the study of Lagrangian Flow Networks, in particular with the concept of Most-Probable-Path-betweenness. This diagnostic identifies the choke points in the topology of a flow system. These, nonetheless, are not necessarily spots of major water passage.

Furthermore, to our knowledge, current notions do not solve the problem of displaying and sorting a series of stations in order to answer the two questions mentioned above. To address these issues, we introduce here a new diagnostic, the crossroadness, which measures the water surface flowing in the neighborhood of a point in a given time window. This permits us to develop a ranking method that estimates the places where the majority of the flux passes, and that at the same time sees waters coming from different locations.

This allows us to design an optimal monitoring system, because each station identified in this way intercepts independent patches of water. We stress that this independence is important for retrieval strategies, for example in the recovering of a contaminant. In fact, in that case the series of the recuperation stations has to be set so that each of them recaptures a different portion of the pollutant that is dispersed. Thus, there is no interest that a station monitors again some waters that have already been intercepted upstream by another one. The same logic is valid in sampling strategies, in which the analysis of the largest surface possible is preferred, and in which sampling twice the same portion of water may be a waste of resources. We stress that the same methodology developed here can be applied to the recently introduced *mixing potential* of Rypina

and Pratt (2017) with the only difference that then the optimality results would correspond to drifting observatories, instead of stations fixed in space.

Reversing the analysis backward in time we can instead quantify, for each point of the domain, the amount of surface that, passing nearby, will feed a target region. In this case the ranking method identifies the major “source” points from which the water distributes over a vast surface, with each source “irrigating” different areas. The independence of the destinations allows us to maximize the surface covered with a minimal identification of source stations. This is an important factor for the assessment of vulnerable points whose contamination can lead serious damages: for instance, for the protection of marine areas or hotspots of biological importance, like a region with a recurrent bloom that sustains the local trophic chain. In those cases, it is central to determine the main sites upstream feeding the whole areas.

We validate the forward-in-time case by analyzing the trajectories of 43 SVP drifters from KEOPS2 campaign. We assess that 6 stations computed with the crossroadness would have been able to intercept on average about the double of the drifters captured with a regular grid, using the same number of detecting sites. Interestingly, the ratio seem to improve when diminishing the detection range. We then studied the persistence of an optimal crossroadness network, by looking at how its intercepting capacity degrades when the network is computed from a velocity field previous to the one that disperses the tracer. Even in this case, the crossroadness stations show better performances than regular grids. This is valid also when we consider a region with stronger turbulence. These facts demonstrate how stations computed from past velocity fields can be applied to future circulation patterns, and validate furthermore the algorithm proposed.

We use the backward-in-time method to analyse the Kerguelen spring primary production during November-December 2011, showing that about the 70% of the waters that supported the bloom had passed in the vicinity of just 3 sites on the Kerguelen plateau during the previous 6 months, in proximity of the Gallieni Spur.

There is a number of cases in which the crossroadness and the ranking method can be applied, and we list here some. For the dispersion of pollutants, the forward in time crossroadness allows us to estimate the most important points in which position a fix station in order to retrieve the contaminant. The aforementioned method can also be used for sampling strategies in order to maximize the surface intercepted and the probability of encountering elements of interest. In search and rescue operations, if the exact missing point is lacking, and the information available is just on the area of disappearance, computing the forward CR could establish optimal observing stations to look for the lost target. Note that in this case, the detection range is explicitly taken into account by our method. Regarding the backward calculation, this can be used for prioritizing survey locations upstream to vulnerable regions (like marine protected areas), or identifying most likely hotspots close to the shore from which fish larvae may span to a large recruiting area.

Computing crossroadness requires the integration of a number of trajectories. We show in Appendix B that, under particular conditions, there is a relationship of the CR with rather direct diagnostics such as the mean absolute velocity or the mean kinetic energy. This then provides a simpler way of calculation, although it does not contain all the information of the original methodology nor it is always valid.

## Acknowledgements

This work is a contribution to the CNES/TOSCA project LAECOS and BIOS-WOT, and it was partly funded by the Copernicus Marine Environment Monitoring Service (CMEMS) Sea Level Thematic Assembly Centre (SL-TAC). C.L and E. H-G. acknowledge support from Ministerio de Economía y Competitividad and Fondo Europeo de Desarrollo Regional through the LAOP project (CTM2015-66407-P, MINECO/FEDER). The authors thank also Isabelle Pujol and Malcolm O'Toole for their helpful advices.

## Appendix A. Temporal persistence of the CR stations along the year

In this Appendix we extend the analysis of Subsec. 3.3 on the possibility of using known velocity fields from the past to obtain sets of CR stations able to monitor transport by future velocity fields.

### *Drifters intercepted with stations computed along the year.*

The SVP drifters release region  $\mathcal{R}_P$  is advected taking as starting day  $D_0$  January, 11th, 2011, for a period  $\tau$  of 30 and 60 days, from which 6 CR stations were calculated. They are then used to see how many real drifters from the dataset released on November 2011 they would have intercepted. The computation is repeated changing  $D_0$ , using each time a different month until December, 2011. The results, reported in Fig. A.1, show a better performance of the CR stations compared to the regular grid, along all the year, with a number of drifters intercepted always higher except for one case (August 2011,  $\tau = 60$  days). The case of 60 days advection presents a linear decrease of drifters intercepted for calculations using the three months previous to November, and then a regular increase again, showing a sort of annual cycle, while the 30 days results seem to show a more irregular trend.

### *Surface monitored with stations computed along the year.*

As in the former case, the region  $\mathcal{R}_P$  is advected starting from  $D_0$  January, 11th, 2011, for a period  $\tau$  of 30 and 60 days, and 6 CR stations were computed. This time the stations are not used to see how many SVP drifters they would have collected, but how many trajectories of the set  $\mathcal{T}(\mathcal{R})_{D_R \rightarrow D_R + \tau}$ , with  $D_R =$  November, 11th, 2011, they would have intercepted.  $D_0$  is varied taking each time the 11th day of a different month of 2011.

The results are reported in Fig. A.2 and display in both cases a temporal decrease of the surface sampled with the CR stations for the first three months. Generally, the surface monitored with this method is about 15% greater than with a regular grid.

## Appendix B. Relation with absolute velocity and mean Kinetic energy

We have described in the main text a way to define and compute the crossroadness at each point of an *observational grid*. This involves the integration forward or backward in time of a large number of initial positions. Although this is not too difficult, it would be desirable to have simpler methodologies, or relationships of CR with other simpler diagnostics. Here we show that, under some circumstances (but not always), CR is large where the modulus of the velocity or the flow kinetic energy is large. When this relationship holds, the qualitative features of the crossroadness become much simpler to find.

To show the above, we note that every circle of radius  $\sigma$  around an observational station presents a cross section (more properly a cross-length)  $2\sigma$  perpendicular to the flow coming from any direction. If  $\sigma$  is sufficiently small to allow considering the velocity field constant on the whole observational circle, the amount of surface crossing that station in a short interval of time  $dt$  is  $2\sigma|v|dt$ , with  $|v|$  the velocity modulus at the station. Integrating during a time  $\tau$  we find that the CR at that point can be written as

$$CR = \int_{D_0}^{D_0+\tau} 2\sigma|v|dt = 2\sigma\tau \langle |v| \rangle, \quad (\text{B.1})$$

with  $\langle |v| \rangle$  the temporal average of the speed  $|v|$  in the time interval  $\tau$ . This formula is the announced approximate relationship between the crossroadness

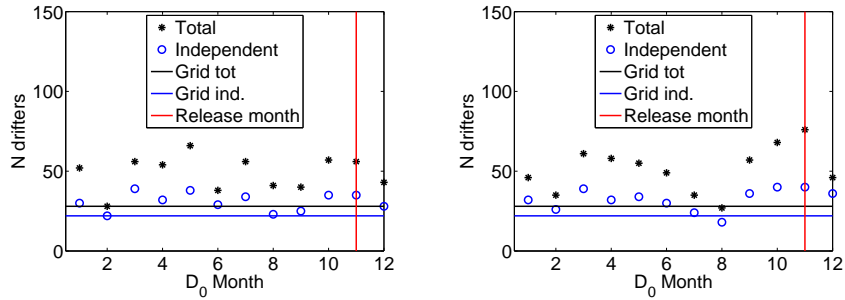


Fig. A.1: Number of drifters intercepted using the different months along the year.  $\delta = \sigma = 0.2^\circ$ . Left panel:  $\tau = 30 \text{ days}$ . Right panel:  $\tau = 60 \text{ days}$ . Horizontal lines: values obtained with a regular grid, total (black) and independent (blue line). Note that the release period of the drifters is November 2011.

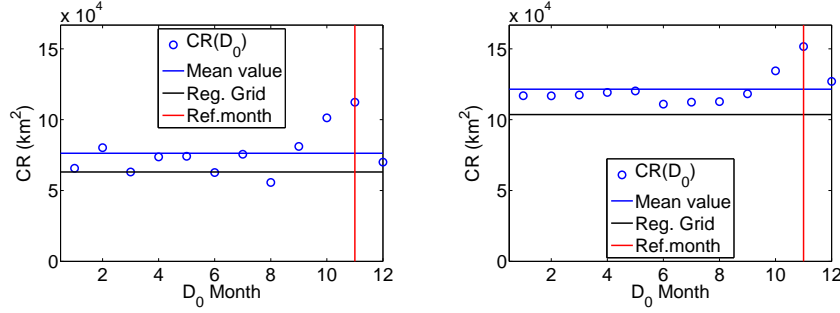


Fig. A.2: Surface of  $\mathcal{R}_P$ , advected from  $D_R = \text{November, 11th, 2011}$ , monitored using the stations computed with velocity currents of different months along the year.  $\delta = 0.1^\circ$ ,  $\tau = 60 \text{ days}$ . Left panel:  $\sigma = 0.1^\circ$ . Right panel:  $\sigma = 0.2^\circ$ . Horizontal lines: surface of November monitored using a regular grid (black line) or 6 CR stations (blue line, mean value of the blue circles)

and the flow speed. Note that we have made no reference to the origin of the water being counted in Eq. (B.1). We expect it to be valid (besides of the restriction on the smallness of  $\sigma$ ) only when the density of tracers over the observational grid is sufficiently homogeneous. This is usually true, for the incompressible flows typical of ocean dynamics, when the initialization grid is much larger than the observational grid, and the former covers most of the later under advection. If in addition to these assumptions the temporal fluctuations of  $|v|$  during the time interval  $\tau$  can be neglected, i.e.  $\langle v^2 \rangle \approx \langle |v| \rangle^2$  then a relationship with the temporal average of the kinetic energy per unit of mass of the flow,  $\langle E_K \rangle = \langle v^2/2 \rangle$ , would hold:

$$CR \approx 2\sigma\tau\sqrt{2 \langle E_K \rangle} \quad (\text{B.2})$$

A validation of Eqs. (B.1) and (B.2) is reported in Fig. B.1, where a map of crossroadness, of kinetic energy and of absolute velocity field, averaged for the month of November, are reported. There, the patterns look pretty identical. This is confirmed by the scatter plot of Fig. B.2, in which the expressions (B.1) and (B.2) are represented by the red line. The correlation coefficients of the two plots are very similar, confirming the validation of the assumptions leading to these equations.

Nevertheless, the kinetic energy or speed present two main differences with the crossroadness, that make them less suitable for monitoring purposes in dispersion problems. In fact, even if these quantities are very similar to CR when the advected area is larger than the domain of calculation, this ceases to be true for smaller advected domains. This is seen in Fig. B.1, lower right panel. There, the crossroadness is computed with the same parameters as in the left upper panel ( $\tau = 30 \text{ days}$ ,  $\delta = \sigma = 0.1^\circ$ ) and on the same *observational grid*, but the *initialization grid* is the one used Subsec. 3.1, i.e. much smaller than the observational one. We can notice that the two patterns differ radically, confirming

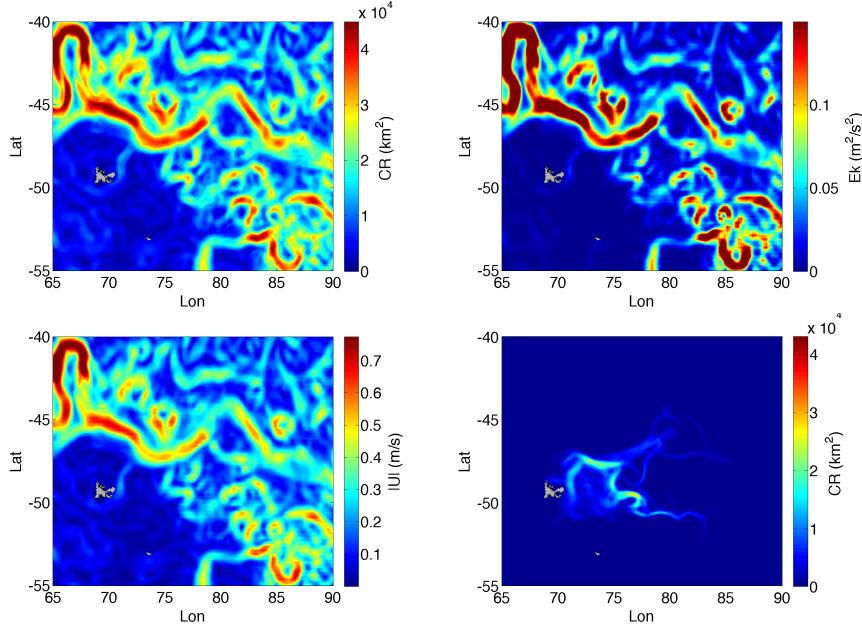


Fig. B.1: Top left panel: crossroadness relative to November 2011 computed with an advection time  $\tau = 30$  days,  $\delta = \sigma = 0.1^\circ$ . Top right panel: mean kinetic energy  $\langle E_K \rangle$  of November 2011. Lower left panel: mean absolute velocity field  $\langle |v| \rangle$  of November 2011. Lower right panel: CR field computed over the same *observational grid* as in the left upper panel, with same parameters, but the *initialization grid* is only the drifter release region (*rectangle* of longitude:  $[70, 75]^\circ$  and latitude:  $[-51, -47]^\circ$ ) as in Subsec. 3.1

the importance of the fulfillment of the hypothesis leading to Eqs. B.1 and B.2. Furthermore, simple maps of kinetic energy or speed do not allow to track the origin of the particles that passed in each point, and thus to establish a hierarchy of importance for observing stations.

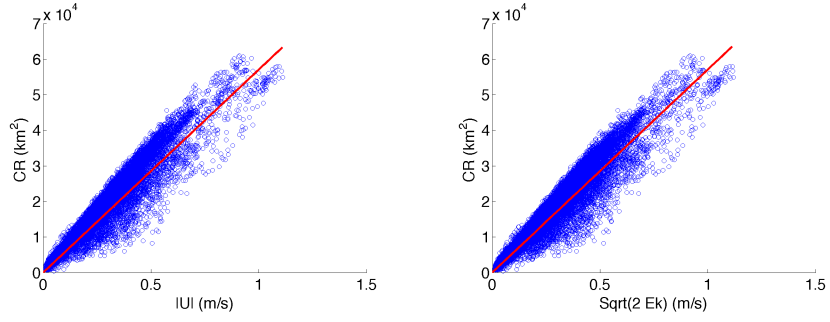


Fig. B.2: Scatterplot of values of CR vs  $\langle |v| \rangle$  (left panel, correlation coefficient: 0.969) and CR vs  $\sqrt{2 \langle E_K \rangle}$  (right panel, correlation coefficient: 0.967) of Fig. B.1

## Bibliography

- Abraham, E.R., Bowen, M.M., 2002. Chaotic stirring by a mesoscale surface-ocean flow. *Chaos: An Interdisciplinary Journal of Nonlinear Science*, 12:373–381. doi:<https://doi.org/10.1063/1.1481615>. PMID: 12779567.
- Andrello, M., Mouillot, D., Beuvier, J., Albouy, C., Thuiller, W., Manel, S., 2013. Low connectivity between mediterranean marine protected areas: A biophysical modeling approach for the dusky grouper *epinephelus marginatus*. *PLOS ONE*, 8:1–15. doi:10.1371/journal.pone.0068564.
- Bellingham, J.G., Willcox, J.S., 1996. Optimizing AUV oceanographic surveys. *Proceedings of Symposium on Autonomous Underwater Vehicle Technology*, pages 391–398. doi:<http://dx.doi.org/10.1109/AUV.1996.532439>.
- Berline, L., Rammou, A.M., Doglioli, A., Molcard, A., Petrenko, A., 2014. A connectivity-based eco-regionalization method of the mediterranean sea. *PLOS ONE*, 9:1–9. doi:10.1371/journal.pone.0111978.
- Blain, S., Sarthou, G., Laan, P., 2008. Distribution of dissolved iron during the natural iron-fertilization experiment KEOPS (Kerguelen Plateau, Southern Ocean). *Deep Sea Research Part II: Topical Studies in Oceanography*, 55:594–605. doi:<https://doi.org/10.1016/j.dsr2.2007.12.028>.
- Boffetta, G., Lacorata, G., Redaelli, G., Vulpiani, A., 2001. Detecting barriers to transport: a review of different techniques. *Physica D: Nonlinear Phenomena*, 159:58–70. doi:[http://dx.doi.org/10.1016/S0167-2789\(01\)00330-X](http://dx.doi.org/10.1016/S0167-2789(01)00330-X).
- Boyd, P.W., Jickells, T., Law, C.S., Blain, S., Boyle, E.A., Buesseler, K.O., Coale, K.H., Cullen, J.J., de Baar, H.J.W., Follows, M., Harvey, M., Lancelot, C., Levasseur, M., Owens, N.P.J., Pollard, R., Rivkin, R.B., Sarmiento, J., Schoemann, V., Smetacek, V., Takeda, S., Tsuda, A., Turner, S., Watson, A.J., 2007. Mesoscale Iron Enrichment Experiments 1993-2005: Synthesis and Future Directions. *Science*, 315:612–617. doi:<http://dx.doi.org/10.1126/science.1131669>.
- Bradbury, I.R., Laurel, B., Snelgrove, P.V., Bentzen, P., Campana, S.E., 2008. Global patterns in marine dispersal estimates: the influence of geography, taxonomic category and life history. *Proceedings of the Royal Society of London B: Biological Sciences*, 275:1803–1809. doi:<http://dx.doi.org/10.1098/rspb.2008.0216>.
- Bray, L., Kassis, D., Hall-Spencer, J., 2017. Assessing larval connectivity for marine spatial planning in the Adriatic. *Marine Environmental Research*, 125:73 – 81. doi:<https://doi.org/10.1016/j.marenvres.2017.01.006>.
- Christaki, U., Obernosterer, I., Van Wambeke, F., Veldhuis, M., Garcia, N., Catala, P., 2008. Microbial food web structure in a naturally iron-fertilized area in the Southern Ocean (Kerguelen Plateau). *Deep Sea Research Part II: Topical Studies in Oceanography*, 55:706–719. doi:<https://doi.org/10.1016/j.dsr2.2007.12.009>.
- Ciappa, A., Costabile, S., 2014. Oil spill hazard assessment using a reverse trajectory method for the Egadi marine protected area (Central Mediterranean

- Sea). *Marine Pollution Bulletin*, 84:44 – 55. doi:<https://doi.org/10.1016/j.marpolbul.2014.05.044>.
- d’Ovidio, F., De Monte, S., Della Penna, A., Cotté, C., Guinet, C., 2013. Ecological implications of eddy retention in the open ocean: a Lagrangian approach. *Journal of Physics A: Mathematical and Theoretical*, 46:254023. doi:10.1088/1751-8113/46/25/254023.
- d’Ovidio, F., Della Penna, A., Trull, T.W., Nencioli, F., Pujol, M.I., Rio, M.H., Park, Y.H., Cotté, C., Zhou, M., Blain, S., 2015. The biogeochemical structuring role of horizontal stirring: Lagrangian perspectives on iron delivery downstream of the Kerguelen plateau. *Biogeosciences*, 12:5567–5581. doi:<https://doi.org/10.5194/bg-12-5567-2015>.
- d’Ovidio, F., Fernández, V., Hernández-García, E., López, C., 2004. Mixing structures in the Mediterranean Sea from finite-size Lyapunov exponents. *Geophysical Research Letters*, 31. doi:<http://dx.doi.org/10.1029/2004GL020328>.
- Dubois, M., Rossi, V., Ser-Giacomi, E., Arnaud-Haond, S., López, C., Hernández-García, E., 2016. Linking basin-scale connectivity, oceanography and population dynamics for the conservation and management of marine ecosystems. *Global Ecology and Biogeography*, 25:503–515. doi:<https://doi.org/10.1111/geb.12431>.
- Eckart, C., 1948. An analysis of the stirring and mixing processes in incompressible fluids. *Journal of Marine Research*, 7:265–275.
- Froyland, G., Padberg, K., England, M.H., Treguier, A.M., 2007. Detection of Coherent Oceanic Structures via Transfer Operators. *Phys. Rev. Lett.*, 98:224503. doi:10.1103/PhysRevLett.98.224503.
- Froyland, G., Stuart, R.M., van Sebille, E., 2014. How well-connected is the surface of the global ocean? *Chaos: An Interdisciplinary Journal of Nonlinear Science*, 24:033126. doi:10.1063/1.4892530.
- Fujiwara, N., Kirchen, K., Donges, J.F., Donner, R.V., 2017. A perturbation-theoretic approach to Lagrangian flow networks. *Chaos*, 27:035813. doi:10.1063/1.4978549.
- Garrett, C., 1983. On the initial streakiness of a dispersing tracer in two-and three-dimensional turbulence. *Dynamics of Atmospheres and Oceans*, 7:265–277. doi:[https://doi.org/10.1016/0377-0265\(83\)90008-8](https://doi.org/10.1016/0377-0265(83)90008-8).
- Hadjighasem, A., Karrasch, D., Teramoto, H., Haller, G., 2016. Spectral-clustering approach to Lagrangian vortex detection. *Physical Review E*, 93:063107. doi:10.1103/PhysRevE.93.063107.
- Haller, G., 2015. Lagrangian coherent structures. *Annual Review of Fluid Mechanics*, 47:137–162. doi:<https://doi.org/10.1146/annurev-fluid-010313-141322>.
- Iacobello, G., Scarsoglio, S., Ridolfi, L., 2018. Visibility graph analysis of wall turbulence time-series. *Physics Letters A*, 382:1 – 11. doi:<https://doi.org/10.1016/j.physleta.2017.10.027>.
- Lam, P.J., Bishop, J.K., 2008. The continental margin is a key source of iron to the HNLC North Pacific Ocean. *Geophysical Research Letters*, 35. doi:<http://dx.doi.org/10.1029/2008GL033294>.

- Lehahn, Y., d'Ovidio, F., Lévy, M., Heifetz, E., 2007. Stirring of the northeast Atlantic spring bloom: A Lagrangian analysis based on multisatellite data. *Journal of Geophysical Research*, 112:C08005. doi:http://dx.doi.org/10.1029/2006JC003927.
- Lindner, M., Donner, R.V., 2017. Spatio-temporal organization of dynamics in a two-dimensional periodically driven vortex flow: A Lagrangian flow network perspective. *Chaos: An Interdisciplinary Journal of Nonlinear Science*, 27:035806. doi:https://doi.org/10.1063/1.4975126.
- Mancho, A., Small, D., Wiggins, S., 2004. Computation of hyperbolic trajectories and their stable and unstable manifolds for oceanographic flows represented as data sets. *Nonlinear Processes in Geophysics*, 11:17–33.
- Martin, P., Loeff, M.R., Cassar, N., Vandromme, P., d'Ovidio, F., Stemmann, L., Rengarajan, R., Soares, M., González, H.E., Ebersbach, F., Lampitt, R.S., Sanders, R., Barnett, B.A., Smetacek, V., Naqvi, S.W.A., 2013. Iron fertilization enhanced net community production but not downward particle flux during the Southern Ocean iron fertilization experiment LOHAFEX. *Global Biogeochemical Cycles*, 27:871–881. doi:http://dx.doi.org/10.1002/gbc.20077.
- McAdam, R., van Sebille, E., 2018. Surface Connectivity and Inter-ocean Exchanges From Drifter-Based Transition Matrices. *Journal of Geophysical Research: Oceans*, pages n/a–n/a. doi:10.1002/2017JC013363.
- Melià, P., Schiavina, M., Rossetto, M., Gatto, M., Fraschetti, S., Casagrandi, R., 2016. Looking for hotspots of marine metacommunity connectivity: a methodological framework. *Scientific Reports*, 6:23705.
- Miron, P., Beron-Vera, F.J., Olascoaga, M.J., Sheinbaum, J., Pérez-Brunius, P., Froyland, G., 2017. Lagrangian dynamical geography of the Gulf of Mexico. *Scientific reports*, 7:7021.
- Monroy, P., Rossi, V., Ser-Giacomi, E., López, C., Hernández-García, E., 2017. Sensitivity and robustness of larval connectivity diagnostics obtained from Lagrangian Flow Networks. *ICES Journal of Marine Science*, 74:1763–1779. doi:http://dx.doi.org/10.1093/icesjms/fsw235.
- Mooers, C., Meinen, C., Baringer, M., Bang, I., Rhodes, R., Barron, C.N., Bub, F., 2005. Cross validating ocean prediction and monitoring systems. *Eos, Transactions American Geophysical Union*, 86:269–273. doi:http://dx.doi.org/10.1029/2005EO290002.
- Okubo, A., 1978. Horizontal Dispersion and Critical Scales for Phytoplankton Patches. *Spatial pattern in plankton communities*, 3:21–42. doi:10.1007/978-1-4899-2195-6.2.
- Ottino, J.M., 1989. The kinematics of mixing: stretching, chaos, and transport, volume 3 of *Cambridge Texts in Applied Mathematics*. Cambridge University Press.
- Padberg-Gehle, K., Schneide, C., 2017. Network-based study of Lagrangian transport and mixing. *Nonlinear Processes in Geophysics*, 24:661–671.
- Park, Y.H., Durand, I., Kestenare, E., Rougier, G., Zhou, M., d'Ovidio, F., Cotté, C., Lee, J.H., 2014. Polar Front around the Kerguelen Islands: An up-to-date determination and associated circulation of surface/subsurface waters.

- Journal of Geophysical Research: Oceans, 119:6575–6592. doi:<http://dx.doi.org/10.1002/2014JC010061>.
- Phillips, J.D., Schwanghart, W., Heckmann, T., 2015. Graph theory in the geosciences. *Earth-Science Reviews*, 143:147 – 160. doi:<https://doi.org/10.1016/j.earscirev.2015.02.002>.
- Planes, S., Jones, G.P., Thorrold, S.R., 2009. Larval dispersal connects fish populations in a network of marine protected areas. *Proceedings of the National Academy of Sciences*, 106:5693–5697. doi:<http://dx.doi.org/10.1073/pnas.0808007106>.
- Prants, S., Budyansky, M., Uleysky, M.Y., 2014a. Identifying Lagrangian fronts with favourable fishery conditions. *Deep Sea Research Part I: Oceanographic Research Papers*, 90:27–35. doi:<https://doi.org/10.1016/j.dsr.2014.04.012>.
- Prants, S., Budyansky, M., Uleysky, M.Y., 2014b. Lagrangian fronts in the ocean. *Izvestiya, Atmospheric and Oceanic Physics*, 50:284–291. doi:<https://doi.org/10.1134/S0001433814030116>.
- Pujol, M.I., Faugère, Y., Taburet, G., Dupuy, S., Pelloquin, C., Ablain, M., Picot, N., 2016. DUACS DT2014: the new multi-mission altimeter data set reprocessed over 20 years. *Ocean Science*, 12:1067–1090. doi:<https://doi.org/10.5194/os-12-1067-2016>.
- Rodríguez-Méndez, V., Ser-Giacomi, E., Hernández-García, E., 2017. Clustering coefficient and periodic orbits in flow networks. *Chaos: An Interdisciplinary Journal of Nonlinear Science*, 27:035803. doi:<https://doi.org/10.1063/1.4971787>.
- Rossi, V., Ser-Giacomi, E., López, C., Hernández-García, E., 2014. Hydrodynamic provinces and oceanic connectivity from a transport network help designing marine reserves. *Geophysical Research Letters*, 41:2883–2891.
- Rypina, I.I., Pratt, L.J., 2017. Trajectory encounter volume as a diagnostic of mixing potential in fluid flows. *Nonlinear Processes in Geophysics*, 24:189. doi:<https://doi.org/10.5194/npg-24-189-2017>.
- Ser-Giacomi, E., Rodríguez-Méndez, V., López, C., Hernández-García, E., 2017. Lagrangian Flow Network approach to an open flow model. *The European Physical Journal Special Topics*, 226:2057–2068. doi:<https://doi.org/10.1140/epjst/e2017-70044-2>.
- Ser-Giacomi, E., Rossi, V., López, C., Hernández-García, E., 2015a. Flow networks: A characterization of geophysical fluid transport. *Chaos: An Interdisciplinary Journal of Nonlinear Science*, 25:036404. doi:<https://doi.org/10.1063/1.4908231>.
- Ser-Giacomi, E., Vasile, R., Hernández-García, E., López, C., 2015b. Most probable paths in temporal weighted networks: An application to ocean transport. *Physical Review E*, 92:012818. doi:[10.1103/PhysRevE.92.012818](https://doi.org/10.1103/PhysRevE.92.012818).
- Ser-Giacomi, E., Vasile, R., Recuerda, I., Hernández-García, E., López, C., 2015c. Dominant transport pathways in an atmospheric blocking event. *Chaos: An Interdisciplinary Journal of Nonlinear Science*, 25:087413. doi:[10.1063/1.4928704](https://doi.org/10.1063/1.4928704).
- Sundermeyer, M.A., Price, J.F., 1998. Lateral mixing and the North Atlantic Tracer Release Experiment: Observations and numerical simulations of La-

- grangian particles and a passive tracer. *Journal of Geophysical Research: Oceans*, 103:21481–21497. doi:<http://dx.doi.org/10.1029/98JC01999>.
- Suneel, V., Ciappa, A., Vethamony, P., 2016. Backtrack modeling to locate the origin of tar balls depositing along the west coast of India. *Science of The Total Environment*, 569-570:31 – 39. doi:<https://doi.org/10.1016/j.scitotenv.2016.06.101>.
- Vrana, B., Allan, I.J., Greenwood, R., Mills, G.A., Dominiak, E., Svensson, K., Knutsson, J., Morrison, G., 2005. Passive sampling techniques for monitoring pollutants in water. *TrAC Trends in Analytical Chemistry*, 24:845–868. doi:<https://doi.org/10.1016/j.trac.2005.06.006>.
- Wiggins, S., 2005. The dynamical systems approach to Lagrangian transport in oceanic flows. *Annual Review of Fluid Mechanics*, 37:295–328. doi:<https://doi.org/10.1146/annurev.fluid.37.061903.175815>.